A New Approach to Sequential Gaussian Simulation with a Trend: Non-Stationary Transformation Tables

E. Gonzales*, Jason A. McLennan**and Clayton V. Deutsch**

*Maptek, Cancun – Quintana Roo, Mexico
**Centre of Computational Geostatistics, University of Alberta

Trends are essential features of geological variables; stationarity only applies to our synthetic random function models. An important goal of research in geostatistics is the search for ways to make random function models better reproduce realistic patterns of natural variability. This paper offers a novel locally varying or non-stationary transformation technique for automatically incorporating the trend within a simulation framework. The definition of a trend, some trend modeling principles, and various trend modeling techniques are discussed. The technique is described and implemented with an example. Additional development is required; however, trends are indeed reproduced in the simulated realizations.

Introduction

The spatial distribution of a geological variable is of dual character: partly structured and partly stochastic [1]. The structured component manifests from a particular sequence of depositional events that control the variable of interest; the stochastic component is due to natural variations in these geological formation processes. This notion of dual character can be represented analytically. The typical decomposition technique calls for dissociation of the $Z(\mathbf{u})$ random function (RF) into separate structured and random components as follows:

$$Z(\mathbf{u}) = m(\mathbf{u}) + R(\mathbf{u}) \tag{1}$$

where $m(\mathbf{u})$ is the structured component or trend and $R(\mathbf{u})$ is the random component or residual. Figure 1 illustrates this simple decomposition for a fining upward log porosity profile. The trend $m(\mathbf{u})$ is a smooth locally varying expectation in the attribute of interest. The decision to split the spatial variability observed into a smoothly varying deterministic trend component and a more erratic or stochastic residual component is arbitrary [2]. Although there are sound geological reasons to dissociate smooth $m(\mathbf{u})$ and random $R(\mathbf{u})$ components from $Z(\mathbf{u})$, the additive decomposition in (1) is arbitrary and not necessarily consistent with or motivated by geological interpretations. The motivation for adopting the particular RF formalism and decomposition in (1) lies, instead, in its convenience. Other breakdown can and should be considered.

Trend Modeling Concepts

Any and all discussions about trends are subjective. This has lead to an extensive variety of trend modeling procedures and methods to account for them throughout industry. However, amidst this large collection of techniques, a few important principles can be discerned. Before describing trend modeling and trend integration techniques, it is useful to clarify these key principles.

Stationarity

It is important to note that special effort is needed to incorporate trends into geostatistical algorithms. Recall the required assumption of stationarity amounting to decide that a particular domain is homogeneous and contains sufficient data for reliable inference of the corresponding stationary RF model $Z(\mathbf{u})$ [3]. Indeed then, it is a significant challenge to integrate deterministic trends $m(\mathbf{u})$ that fundamentally violate any previous assumption of stationarity.

Importance of the Trend

A common concern is when the trend is in fact significant and needs to be modeled and accounted for. This subjective decision depends on the level of deterministic geological knowledge and hard/soft supporting data available. Consider the vertical string of unestimated grid cells a distance $\mathbf{h}$ away from the log porosity profile in Figure 1. The approximate form of the trend $m(\mathbf{u})$ shown in the log porosity profile should be reproduced for any geologically acceptable model of heterogeneity in this string of cells. Choosing not to explicitly model the trend deterministically through $m(\mathbf{u})$ and depending instead on the probabilistic interpolation of only the single string of data, however, may not suitably reproduce $m(\mathbf{u})$. This is especially true if $\mathbf{h}$ is beyond the range of horizontal porosity correlation. In these cases, the trend $m(\mathbf{u})$ must be explicitly modeled in order to be reproduced in estimation and simulation. From the porosity profile and knowledge of some fining upward geological interpretation, the trend component $m(\mathbf{u})$ can be modeled deterministically for the unestimated grid blocks.

In general, a trend model is needed when the resulting models of heterogeneity do not satisfactorily reproduce important large scale geological heterogeneities. And this is often the case in settings where there are very limited sample data coupled with a coherent deterministic geological understanding of the phenomenon.

Balancing Deterministic and Probabilistic Variability

Decomposition of the $Z(\mathbf{u})$ RF according to (1) leads to the following decomposition of total variability in the original $Z(\mathbf{u})$ random variable (RV):

$$C\{Z(\mathbf{u}), Z(\mathbf{u})\} = C\{m(\mathbf{u}), m(\mathbf{u})\} + C\{R(\mathbf{u}), R(\mathbf{u})\} + 2 \cdot C\{m(\mathbf{u}), R(\mathbf{u})\} \qquad (2)$$

The amount of variability modeled by the trend $m(\mathbf{u})$ is a subjective balance between determinism and stochasticity. Deterministic geological interpretations governing the formation of a deposit or reservoir are subjective. In all cases, the trend should model no more variability than what our deterministic understanding of the geological processes suggests; nevertheless, in practice, the trend is often over fit and represents too much variability. That is, the variability captured in the $C(m(\mathbf{u}), m(\mathbf{u}))$ term is artificially high relative to $C(R(\mathbf{u}), R(\mathbf{u}))$. Incorporating too much variability in the trend dangerously leaves too little variability to the random fluctuations inherent in all petrophysical property variables and modeled by stochastic geostatistical methods.

Consider again the estimation scheme in Figure 1. It is assumed that the separation $\mathbf{h}$ is slightly beyond the range of spatial correlation and that there exists some logical rationale for the fining upward trend in porosity at the unestimated grid blocks. An explicit model of $m(\mathbf{u})$ would then be needed since the available porosity profile data on the left will not effectively reproduce the fining upward trend. It is easy to let the neighboring porosity profile over influence the $m(\mathbf{u})$ trend model without any logical incremental deterministic knowledge. This recurring situation is an ongoing challenge in practice.

Scale Dependency

Interpreting and modeling the trend is highly dependent on scale. For example, some smaller elevation intervals on the porosity profile shown in Figure 1 actually show a coarsening with elevation. Some elevation intervals correspond to no trend at all. The interpretation depends on scale. The domain size within which a stationary RF $Z(\mathbf{u})$ is applied then has a significant impact on the trend model $m(\mathbf{u})$.

Trend Modeling Methods

The general approach to trend modeling in three dimensions is to build a 2D aerial trend $m(x,y)$ and 1D vertical trend $m(z)$ separately and then merge them into a full 3D trend $m(x,y,z)$. There are several methods available for generating lower dimension 2D and 1D aerial and vertical trends, each method with its own advantages/disadvantages, implementation details, and range of applicability. Four of the most common trend modeling techniques are listed below with brief descriptions:

1. *Hand Mapping* is the classic approach to trend modeling. Although hand mapping techniques are simple and flexible in allowing the practitioner to model virtually any anticipated smoothly varying spatial structure, these methods are not repeatable and difficult to adjust when faced with new data or information;

2. *Moving Window Averages* standardize the attribute of interest within overlapping regions spanning the full domain. Moving window averages are simple, effective, and easy to implement. The vertical trend is usually calculated with a moving overlapping vertical 1D window/interval average;

3. *Inverse Distance* is a grid estimation/mapping procedure that weights surrounding data inversely to their distance from the estimation location and is a simple and effective trend modeling technique in 2D; and

4. *Kriging* is a linearly weighted least squares error estimation technique and is one of the most effective and robust trend modeling tools available. Different anisotropy, expected values, and levels of variability can be incorporated into the trend model using kriging methods.

An essential guideline for implementing any of these methods for constructing the trend is avoiding the tendency to overestimate its spatial variability in $C(m(\mathbf{u}), m(\mathbf{u}))$. For this reason the classical application of kriging for estimation is different than that for trend modeling. Two popular alternative kriging setups are global kriging where all sample data are retained for every grid cell estimate and block ordinary kriging where a grid cell discretization and significant nugget effect are used. Similarly, inverse distance weighting is implemented with higher than normal inverse distance powers and data to ensure smoothness; large overlapping windows are used for moving window averages; and hand mapping can virtually dial in any level of $m(\mathbf{u})$ variability.

A combination of the methods above are used to construct the trend in the required dimensions. These lower dimensional trends must then be merged into a full 3D $m(x,y,z)$ trend model. The common approach to this problem is assigning the dimensional trend components probabilities and using probability combination schemes [5]. The two most frequently used combination relationships are the full independence and conditional independence (permanence of ratios) schemes [4, 5].

Accounting for the Trend

Geostatistics is increasingly popular for mapping regionalized variables in the mining and petroleum industry. These tools provide the ability to construct multiple equally probable and geologically realistic models of heterogeneity that can honor several types of conditioning information. These models can be used to assess the uncertainty of various production performance variables. Conventional geostatistics will reproduce the sample data, its distribution, and the model of spatial correlation; however, there can often be too few data to satisfactorily reproduce a significant trend. Geostatistical workflows must then be modified to explicitly account for the trend.

There are four currently available approaches to incorporate the trend into geostatistical models of heterogeneity: (1) non-stationary kriging, (2) intrinsic random functions of order k (IRF-k), (3) explicitly modeling $m(\mathbf{u})$ and $R(\mathbf{u})$ separately and recombining, and (4) stepwise transformation of residuals conditional to the trend. These are now reviewed.

Non-Stationary Kriging

The earliest group of approaches aimed at integrating trends into geostatistical estimation is non-stationary kriging. The most popular and well known form of non-stationary kriging is referred to as kriging with a trend (KT), originally identified and developed as universal kriging (UK) by Matheron in 1969 [6]. Here, the trend is modeled as a deterministic function of the coordinates vector $\mathbf{u}$. The KT algorithm provides the least squares error estimation of the functional trend coefficients, the corresponding estimate of the locally varying mean $m^*(\mathbf{u})$, the least squares error estimation of the residuals $r^*(\mathbf{u})$, and the corresponding estimate of the original variable $z^*(\mathbf{u}) = m^*(\mathbf{u}) + r^*(\mathbf{u})$ [7].

However, there are several implementation challenges facing this approach [3, 8]. The following five are the most important:

1. KT is not theoretically correct for the implementation of simulation;

2. It is not the spatial law of the original $Z(\mathbf{u})$ RF that is required to interpolate $z(\mathbf{u})$ data in KT. It is actually the spatial law of $R(\mathbf{u})$ that is required. The usual assumption of stationarity for $Z(\mathbf{u})$ must then be transferred to the residual RF $R(\mathbf{u})$. Inference of this spatial law is difficult since $R(\mathbf{u})$ is not sampled in reality and its realizations are only a product of the artificial construct in (1).

3. Fitting the trend automatically is not recommended due to the possibility of artificial large scale heterogeneity due to limited data for estimating the trend $m(\mathbf{u})$;

4. There are several situations in which the estimation setting creates a singular matrix within the universal kriging system of equations; and

5. The set of n conditioning data retained for the least squares estimation of the mean $m(\mathbf{u})$ is not typically the same as for ordinary and simple kriging in practice.

Geostatistical simulation is theoretically incorrect with any form of kriging other than simple kriging. Subsequent methods to account for the trend focused on theoretically correct integration with simulation.

Intrinsic Random Functions of Order k (IRF-k)

The challenges associated with inferring the residual covariance $R(\mathbf{u})$ for KT methods motivated the consideration and use of intrinsic random functions of order k (IRF-k) [9]. IRF-k are random functions with second-order stationary increments of order k [10]. The generalized covariance (GC) $K(\mathbf{h})$ is the correlation structure of an IRF-k. Conventional geostatistics corresponds to the 0-order ($k = 0$) increments $Z(\mathbf{u} + \mathbf{h}) - Z(\mathbf{u})$ to which the variogram is the GC function $K(\mathbf{h})$. The application of non-stationary kriging with IRF-k is notorious for quite restrictive isotropic $K(\mathbf{h})$ models.

In 1990, Dimitrakopoulos [11] developed and presented a comprehensive step-by-step non-stationary simulation procedure using IRF-k. There are three main steps: (1) on-line unconditional simulation of Wiener-Levy process for the IRF-k in $\boldsymbol{R}^1$, (2) use of the turning-bands method to map the $\boldsymbol{R}^1$ realizations into $\boldsymbol{R}^n$, (3) conditioning to available data with kriging, and (4) verification of the reproduced GC using generalized variograms. Unlike non-stationary kriging using the variogram, the use of GC's from IRF-k yield theoretically correct results in a conditional simulation framework.

Additive Decomposition

The most common approach for integrating the trend into the construction of geological models of heterogeneity is performing geostatistical estimation and simulation of the assumed stationary residuals $R(\mathbf{u})$ after the modeled trend $m(\mathbf{u})$ is subtracted from the original variable $Z(\mathbf{u})$. This straightforward and intuitive procedure nominally reproduces the general form of the trend model $m(\mathbf{u})$; however, there are two practical limitations:

1. The application of parametric geostatistical estimation and simulation tools to the $R(\mathbf{u})$ stationary RF implies that $R(\mathbf{u})$ is independent from $m(\mathbf{u})$, a property referred to as homoscedasticity. However, virtually all scatters of ($r(\mathbf{u})$, $m(\mathbf{u})$) pairs will reveal some structured relational behavior known as heteroscedasticity. Classical geostatistical tools, therefore, must be modified to account for these common departures from homoscedasticity; and

2. The dissociation in (1) constrains $R(\mathbf{u}) \geq m(\mathbf{u})$ for nonnegative RVs $Z(\mathbf{u})$. Modeling the residuals and adding the mean back does not ensure this constraint is satisfied. Again, the classic application of geostatistics must then be modified to account for this constraint.

Stepwise Conditional Transformation

The two problems noted above for the additive decomposition approach are described and motivate the stepwise conditional transformation technique in [12]. The solution proposed when the first of these problems persists is a stepwise transformation of the residual data conditional to the trend. This transformation assumes the following form:

$$Y_R(\mathbf{u}) = G^{-1}\big[F\big(R(\mathbf{u})\,|\,m(\mathbf{u})\big)\big] \tag{3}$$

where $Y_R(\mathbf{u})$ is the Gaussian G transform of the residual random variable $R(\mathbf{u})$ conditional to local $m(\mathbf{u})$ windows. Similarly, the solution when the second of these problems persists is a stepwise transformation of the original variable conditional to the trend:

$$Y_Z(\mathbf{u}) = G^{-1}\big[F\big(Z(\mathbf{u})\,|\,m(\mathbf{u})\big)\big] \tag{4}$$

Both transformations complement conventional practice. The same decomposition in (1) is used in that the trend $m(\mathbf{u})$ and residual $R(\mathbf{u})$ is modeled separately and recomposed. Here, however, a pre (forward) and post (backward) processing stepwise conditional transformation step is implemented in order to preserve heteroscedastic and constraint features. All necessary implementation details as well as mining and petroleum examples are given in [12].

The Non-Stationary Transformation Technique

We develop an alternative to the previous four approaches to accounting for the trend within a geostatistical simulation framework. The method is based on a locally varying (non-stationary) transform (LVT). This LVT concept is embedded within the classical sequential Gaussian simulation (SGS) framework. There are 10 steps to the overall modified SGS methodology, hereafter referred to as SGS-LVT. Each step of the proposed SGS-LVT methodology is now described.

Step I: Collect all relevant hard sample data of the attribute of interest subsequently used to condition the simulations. These data are represented by $z(\mathbf{u}_s)$, $s = 1,\ldots, S$.

Step II: Establish a path through the grid network visiting each node once. The grid node locations are represented by the coordinates vector $\mathbf{u}_n$, $n = 1,\ldots, N$. To avoid artifacts, the path through the N grid nodes should be random [13].

A random path can be created with a basic random number generator. A random number is assigned to each node and sorted in ascending order. A random path is defined by visiting the nodes in this order. Figure 2 illustrates the process within a simple 3 x 3 grid.

Step III: At each of the $\mathbf{u}_n$ node locations, determine the univariate cumulative distribution function (cdf) representative of the local area surrounding the simulation location. These local cdfs are denoted with $F_Z(\mathbf{u}_n; z)$. This step is in fact the fundamental distinction from the traditional implementation of SGS where of course under the assumption of stationarity these cdfs are the same stationary $F_Z(z)$ cdf built from all $z(\mathbf{u}_s)$ data, that is, $F_Z(\mathbf{u}_n; z) = F_Z(z)$ for all $\mathbf{u}_n$, $n = 1,\ldots, N$ grid node locations. When necessary, declustering weights $w^D(\mathbf{u}_s)$ are applied to the $z(\mathbf{u}_s)$ data to attain a more representative $F_Z(z)$ cdf that accounts for sampling bias [14].

The goal here is to relax the assumption of stationarity by considering these non-stationary or locally varying $F_Z(\mathbf{u}_n; z)$ cdfs. All S data are used to construct each of the N $F_Z(\mathbf{u}_n; z)$; however, the weights $w^T(\mathbf{u}_s)$ assigned to the $z(\mathbf{u}_s)$ data are neither equal nor derived from declustering/debiasing. They are derived from one of the previously described trend modeling algorithms. Either the inverse distance (ID) or simple kriging (SK) schemes are used to build the $w^T(\mathbf{u}_s)$ weights in calculating the local $F_Z(\mathbf{u}_n; z)$ cdfs representative of the local area surrounding the $\mathbf{u}_n$ location.

Figure 3 illustrates the concept. There are $S = 10$ $z(\mathbf{u}_s)$ sample data color coded from blue (low values) to red (high values) available within the 2D XY rectangular domain $\mathbf{D}$. Two hand-drawn contour lines separate the domain into high, medium, and low valued areas. There are a total of $N = 117$ (9 x 13) $\mathbf{u}_n$ grid node locations where the local $F_Z(\mathbf{u}_n; z)$ cdfs are required. The conventional SGS approach, under the assumption of stationarity, assumes all $F_Z(\mathbf{u}_n; z)$ are equivalent to the stationary $F_Z(z)$ cdf built from the 10 data weighted equally ($w(\mathbf{u}_s) = 1/S = 1/10$) or by declustering weights ($w(\mathbf{u}_s) = w^D(\mathbf{u}_s)$). The new SGS-LVT approach does not assume stationarity and instead calculates each of the $N = 117$ $F_Z(\mathbf{u}_n; z)$ cdfs differently by weighting the $S = 10$ $z(\mathbf{u}_s)$ with either ID weights $w^{ID}(\mathbf{u}_s)$ or SK weights $w^K(\mathbf{u}_s)$ as if estimating at the yet unknown $\mathbf{u}_n$

location. Using the new SGS-LVT method then, the representative $F_Z(\mathbf{u}_n; z)$ cdfs change according to the location vector $\mathbf{u}_n$. In expected high valued $\mathbf{u}_n$ locations, the $w^{\mathrm{ID}}(\mathbf{u}_s)$ or $w^{\mathrm{K}}(\mathbf{u}_s)$ weights are higher for high $z(\mathbf{u}_s)$ samples and the $F_Z(\mathbf{u}_n; z)$ cdf shifts lower (red in Figure 3); in expected low valued $\mathbf{u}_n$ locations, the $w^{\mathrm{ID}}(\mathbf{u}_s)$ or $w^{\mathrm{K}}(\mathbf{u}_s)$ weights are higher for low $z(\mathbf{u}_s)$ samples and the $F_Z(\mathbf{u}_n; z)$ cdf shifts higher.

Calculating the locally varying $F_Z(\mathbf{u}_n; z)$ cdfs as described above will subsequently account for a locally varying expectation or trend in the attribute of interest. We will see how this develops and carries through later steps. First recall the essential guideline for applying any trend modeling method – avoiding the tendency to overestimate the spatial variability in the trend ($C(m(\mathbf{u}), m(\mathbf{u}))$ in relation (2)) – and the associated ID and SK algorithm changes to respect this guideline. Indeed, this same principle is relevant here when calculating the $w^{\mathrm{ID}}(\mathbf{u}_s)$ or $w^{\mathrm{K}}(\mathbf{u}_s)$ to locally adjust the $F_Z(\mathbf{u}_n; z)$ cdf. For both ID and SK, a global search is used retaining all S sample data. The amount of variability in the trend or the $C(m(\mathbf{u}), m(\mathbf{u}))$ term can then be dialed in with the ID weighting power and SK variogram model.

Figure 4 illustrates the effect increasing the distance power (IDP) for the ID scheme and decreasing the continuity in the variogram for the SK scheme has on the locally varying representative $F_Z(\mathbf{u}_n; z)$ cdfs. For IDP nearly zero and virtually nugget effect variograms, the set of $w(\mathbf{u}_s)$ weights are nearly equal at all $\mathbf{u}_n$ locations, the assumption of stationarity is strong, and the variation between $F_Z(\mathbf{u}_n; z)$ cdfs is minimal. For IDP approximately equal to 0.5 and variograms with approximately 30% nugget and range equivalent to roughly half the domain size ½|$\mathbf{D}$|, the set of $w(\mathbf{u}_s)$ weights change according to $\mathbf{u}_n$ location, the assumption of stationarity is relaxed, and the variation between $F_Z(\mathbf{u}_n; z)$ cdfs increases. For IDP greater than 1.5 and variograms with less than 15% nugget and more than ½|$\mathbf{D}$ for the range, the $w(\mathbf{u}_s)$ weights change drastically with $\mathbf{u}_n$ location, the assumption of stationarity is ignored, and the variation between $F_Z(\mathbf{u}_n; z)$ cdfs is significant.

Step IV: Perform a Gaussian transform of all relevant $z(\mathbf{u}_s)$ sample data and previously simulated values $z^{(l)}(\mathbf{u}_n)$ found within some predefined search space using the local $F_Z(\mathbf{u}_n; z)$ cdf calculated in the prior step as a reference distribution.

The Gaussian transform of a sample $z(\mathbf{u}_s)$ or previously simulated node $z^{(l)}(\mathbf{u}_n)$ is obtained by matching its $F_Z(\mathbf{u}_n; z)$ cdf value to the cdf on a standardized Gaussian distribution G_Y with mean of zero and standard deviation and/or variance of one:

$$y(\mathbf{u}) = G_Y^{-1}\left(F_Z\left(\mathbf{u}_n; z\right)\right) \tag{5}$$

The blue arrow in the top of Figure 5 illustrates this normal score transformation. The set of normal score local conditioning data is denoted $y(\mathbf{u}_c)$, $c = 1,\ldots, C$. Note the changing $F_Z(\mathbf{u}_n; z)$ with location will alter the set of data values $y(\mathbf{u}_c)$ retained for subsequent steps even when the same $z(\mathbf{u}_s)$ and $z^{(l)}(\mathbf{u}_n)$ data are found within the search.

Step V: Build the local conditional cumulative distribution function (ccdf) with SK using the $y(\mathbf{u}_c)$ normal score data from the previous step. The standardized variogram model is inferred from only the original $z(\mathbf{u}_s)$ sample data. The resulting Gaussian ccdf, completely parameterized by the SK estimate $y^*(\mathbf{u}_n)$ and standard deviation $\sigma^*(\mathbf{u}_n)$, is denoted $G_Y(\mathbf{u}_n; y|C)$.

Step IV: Draw a simulated value $y^{(l)}(\mathbf{u}_n)$ from the local ccdf $G_Y(\mathbf{u}_n; y|C)$.

Step VII: Back transform the Gaussian $y^{(l)}(\mathbf{u}_n)$ simulated value to its real unit value $z^{(l)}(\mathbf{u}_n)$ through the inverse local cdf $F_Z^{-1}(\mathbf{u}_n; z)$ as follows:

$$z^{(l)}\left(\mathbf{u}_n\right) = F_Z^{-1}\left(y^{(l)}\left(\mathbf{u}_n\right)\right) \qquad (6)$$

This transformation is represented by the red line in Figure 5. Note the changing $F_Z(\mathbf{u}_n; z)$ cdf with location will result in different $z^{(l)}(\mathbf{u}_n)$ simulated values even when the same normal score simulated value $y^{(l)}(\mathbf{u}_n)$ is calculated.

Step VIII: Add the simulated value $z^{(l)}(\mathbf{u}_n)$ to the pool of conditioning data;

Step IX: Proceed to the next unknown $\mathbf{u}_n$ location according to the previously established random path and loop over steps III to VIII until all N grid nodes have been visited and simulated.

Step X: Repeat steps II through IX to construct multiple $l = 1,\ldots, L$ realizations.

Example

The grades in this example are from a gold deposit. There are 67 available gold samples (oz/t) located on a 2D easting-elevation XZ cross section. Figure 6 shows a histogram and location map of the samples. The gold grade distribution is positively skewed with a mean and variance of 1.36 and 1.72, respectively. The location map reveals a strong non-stationarity or trend of decreasing gold concentration with depth. There is then definitely a need to incorporate a model of the trend into the geostatistical simulation of gold grades since there is insufficient data for reproducing the trend automatically.

For reference, a trend model is generated with a global simple kriging estimation scheme. Three different trend models are created at a 2 x 2m resolution and shown in Figure 7 representing a high (left), medium (middle), and low (right) amount of variability. These models are built using a variogram with zero, 10%, and 50% nugget effects, respectively. The decision to choose one trend model over another is subjective. These trend models are subsequently used as different reference trend models to compare the ability of the SGS-LVT and SGS algorithms to reproduce the trend.

Variography was performed using the normal score values of the 67 gold sample data. The best correlation and principle variogram direction is along the 45° direction in the XZ plane; the minor variogram direction is then 135°. Figure 8 shows the final variogram points and models for both the 45° (red) and 135° (blue) direction. The analytical form of the final variogram model is:

$$\gamma(\mathbf{h}) = 0.35 + 0.55 \cdot Sph(\mathbf{h})_{\substack{a_{45^o}=80m \\ a_{135^o}=60m}} + 0.10 \cdot Sph(\mathbf{h})_{\substack{a_{45^o}=400m \\ a_{135^o}=60m}} \qquad (7)$$

The SGS algorithm is first implemented for comparison to the SGS-LVT approach. The first three realizations and the average of 20 realizations are all shown in Figure 9. Notice the poor reproduction of all the trend models in Figure 7 especially away from data and past the range of correlation represented by the variogram model in Figure 8. This confirms the need for explicitly incorporating a trend model into the simulation.

Figure 10 shows the results of the SGS-LVT method using each level of trend variability in Figure 7. The same zero, 10%, and 50% nugget effect variograms and global kriging routine are used to construct the trend models in Figure 7 are used here to calculate the $w^K(\mathbf{u}_s)$ weights for locally adjusting the $F_Z(\mathbf{u}_n; z)$ cdfs. The first three realizations and the average of 20 realizations are shown for the high (top row), medium (middle row), and low (bottom row) trend variability cases in Figure 10. Notice here the additional control exerted by the locally varying $F_Z(\mathbf{u}_n; z)$ transformation tables on the grades away from data and past the range of correlation represented

by the variogram model in Figure 8. At each level of variability in the trend, the SGS-LVT grade model satisfactorily reproduces the trend.

Conclusion

The SGS-LVT method is a robust simulation-based algorithm capable of accounting for large-scale trends. The methodology and implementation involves a straightforward modification of the traditional SGS algorithm. The amount of variability allocated to the trend is tuned in by the weights used to calculate the local $F_Z(\mathbf{u}_n; z)$ cdfs. An increasingly random spatial law is used for calculating the $F_Z(\mathbf{u}_n; z)$ cdf weights to decrease the influence of the trend and approach the classic assumption of stationarity. The trend is automatically integrated into the simulated values through the locally varying $F_Z(\mathbf{u}_n; z)$ forward transformation for $y(\mathbf{u}_c)$ conditioning data and back transformation for $z^{(l)}(\mathbf{u}_n)$ simulated values.

References

[1] Journel, A.G. and Huijbregts, Ch.J. *Mining Geostatistics*. The Blackburn Press, New Jersey, 1978.

[2] Journel, A.G. and Rossi, M.E. *When do we Need a Trend Model in Kriging?*, Mathematical Geology, vol. 21, no. 7, 1989.

[3] McLennan, J.A. and Deutsch, C.V., *Kriging with a Trend*. CCG Report 8, September 2006.

[4] McLennan, J.A., Leuangthong, O., and Deutsch, C.V., *Trend Modeling Techniques and Guidelines*. CCG Report 7, September 2005.

[5] Journel, A.G. *Combining Knowledge from Diverse Sources: An Alternative to Traditional Data Independence Hypotheses*. Mathematical Geology, Vol. 34, No. 5, July 2002.

[6] Matheron, G. *Le Krigeage Universel: Fascicule 1*. Cahiers du CMM, 1969, 82 p.

[7] McLennan, J.A., Leuangthong, O., and Deutsch, C.V., *Another Look at the Kriging Equations*. CCG Report 8, September 2006.

[8] Armstrong, M. *Problems with Universal Kriging*, Mathematical Geology, 16 (1), 1984, pp. 101-108.

[9] Journel, A.G. *Fundamentals of Geostatistics in Five Lessons*. American Geophysical Union 1989.

[10] Chiles, J. and Delfiner, P. *Geostatistics: Modeling Spatial Uncertainty*. John Wiley & Sons, New York, 1999.

[11] Dimitrakopoulos, R. *Conditional Simulation of Intrinsic Random Functions of Order k*. Mathematical Geology, 22 (3), 1990, pp. 361-380.

[12] Leuangthong, O. and Deutsch, C. V. *Transformation of Residuals to Avoid Artifacts in Geostatistical Modelling with a Trend*, Mathematical Geology, 36 (3), 2004, pp. 287-305.

[13] McLennan, J.A. *A Closer Look at the Path in Sequential Simulation*. CCG Report 4, September 2002.

[14] Pyrcz, M.J. and Deutsch, C.V. *Declustering and Debiasing*. CCG Report 4, 2002.
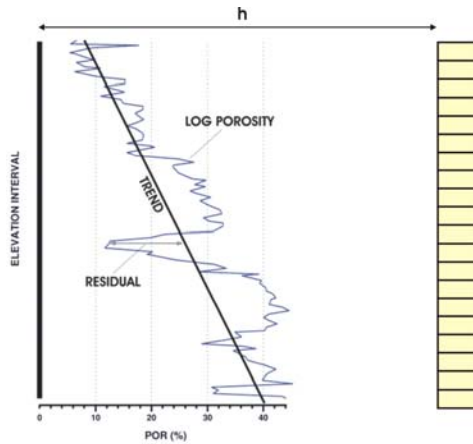
Figure 1: An illustration of the trend $m(\mathbf{u})$ and residual $R(\mathbf{u})$ components of the $Z(\mathbf{u})$ RF for a fining upward porosity profile located along the dark vertical . An unestimated vertical string of 20 grid cells is also shown a distance and direction vector $\mathbf{h}$ away from the porosity profile.
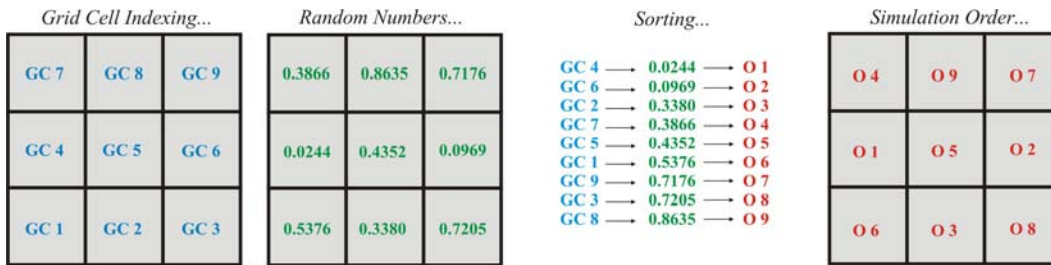

Figure 2: Illustrating the establishment of a random path through a simple 3 x 3 grid using a basic uniform random number generator.
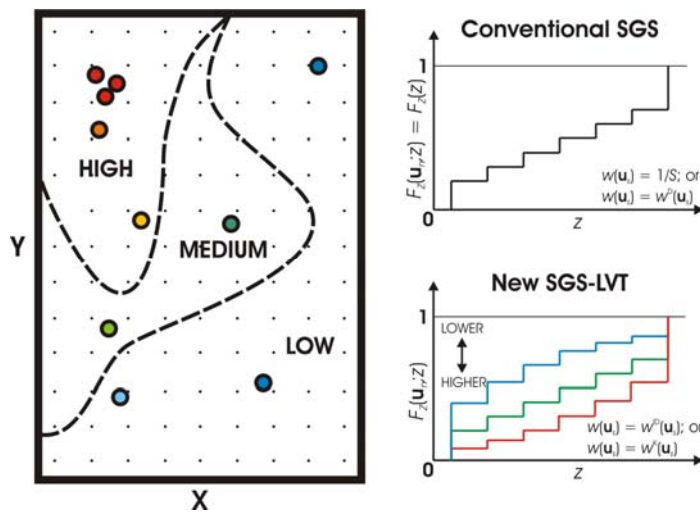

Figure 3: The concept of locally varying representative $F_Z(\mathbf{u}_n; z)$ cdfs.
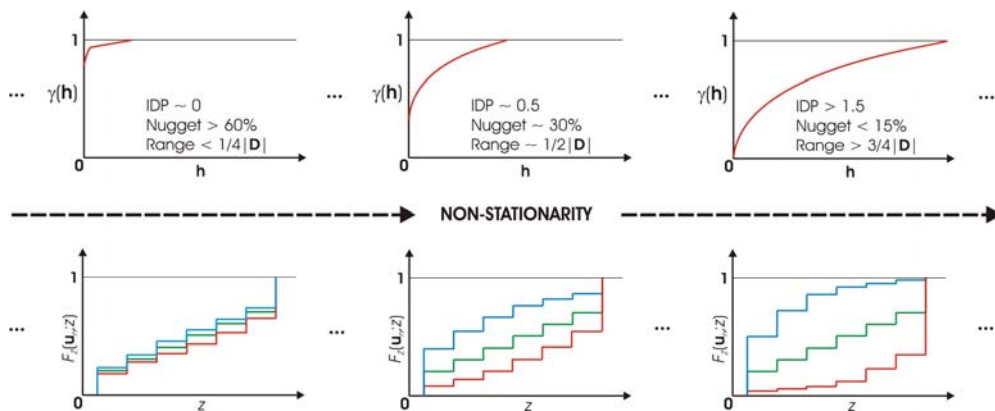
Figure 4: The control of increasing inverse distance powers and spatial correlation in calculating the $w(\mathbf{u}_s)$ weights on the variation of local $F_Z(\mathbf{u}_n; z)$ cdfs between $\mathbf{u}_n$ locations.
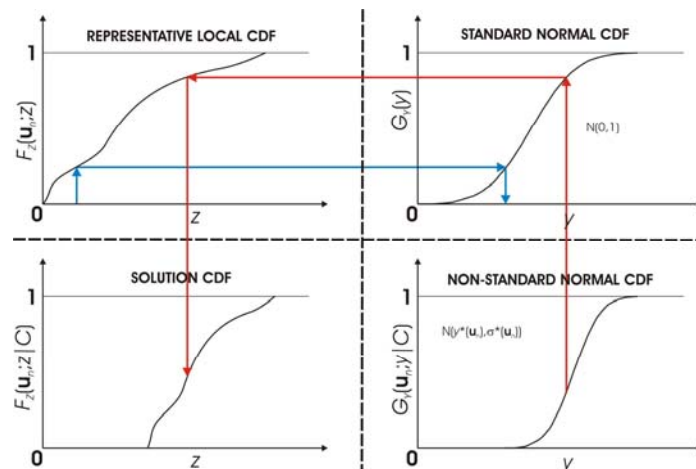

Figure 5: Illustration of the normal score transformation for $y(\mathbf{u}_s)$ conditioning data (blue) and the back transformation of $y^{(l)}(\mathbf{u}_n)$ simulated values to real unit $z^{(l)}(\mathbf{u}_n)$ simulated values.
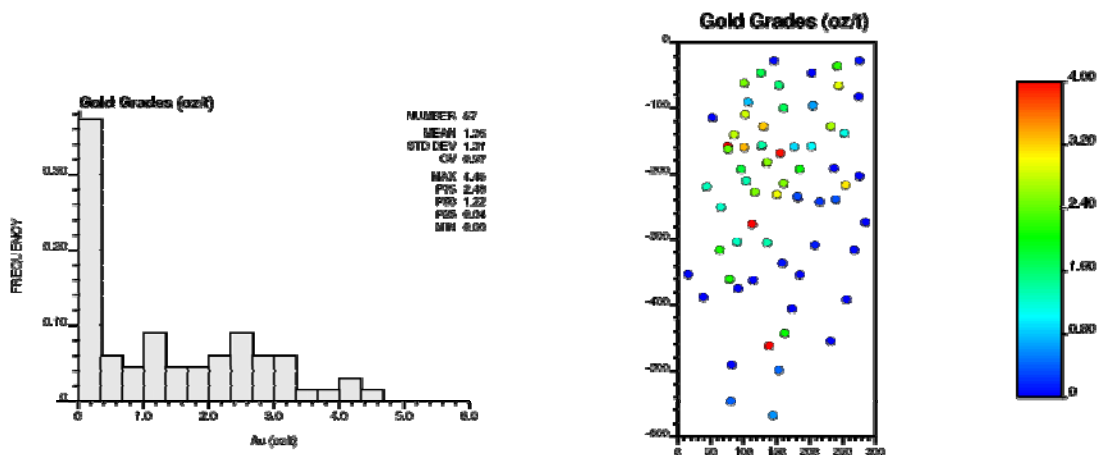

Figure 6: The statistical (histogram - left) and spatial (location map – right) distribution of gold grade used in the example.

120-11
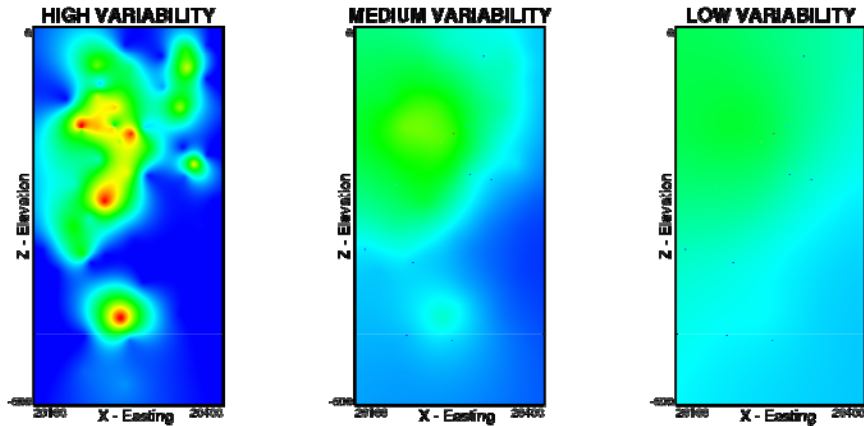
Figure 7: Three trend models with low (left), medium (middle), and high (right) variability created with a global simple kriging scheme. The color scale is the same in Figure 6.
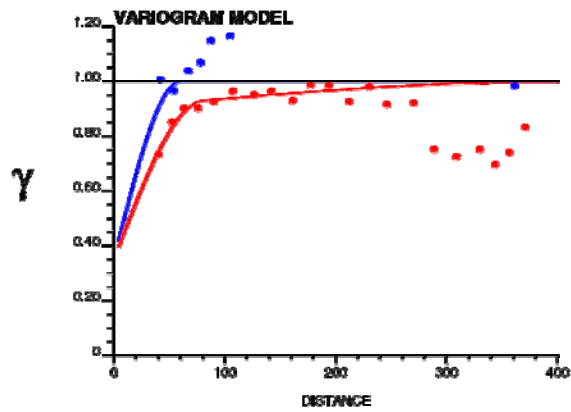
Figure 8: The experimental and model variogram for the major (45°/red) and minor (135°/blue) directions.
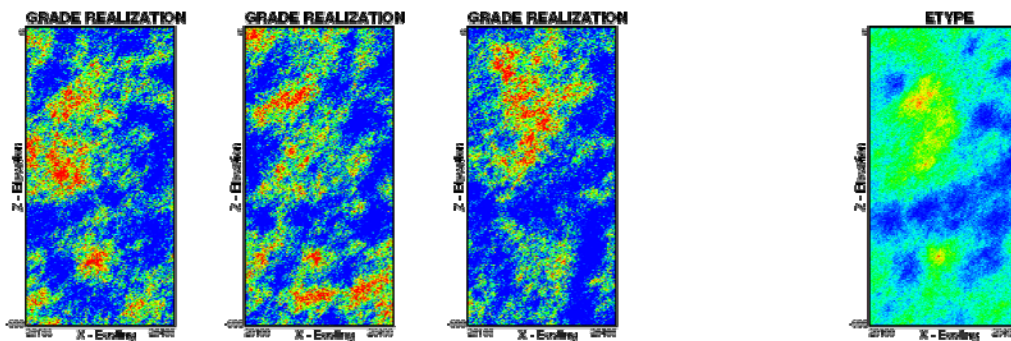
Figure 9: The first 3 SGS realizations and average over 20 realizations showing poor trend reproduction.
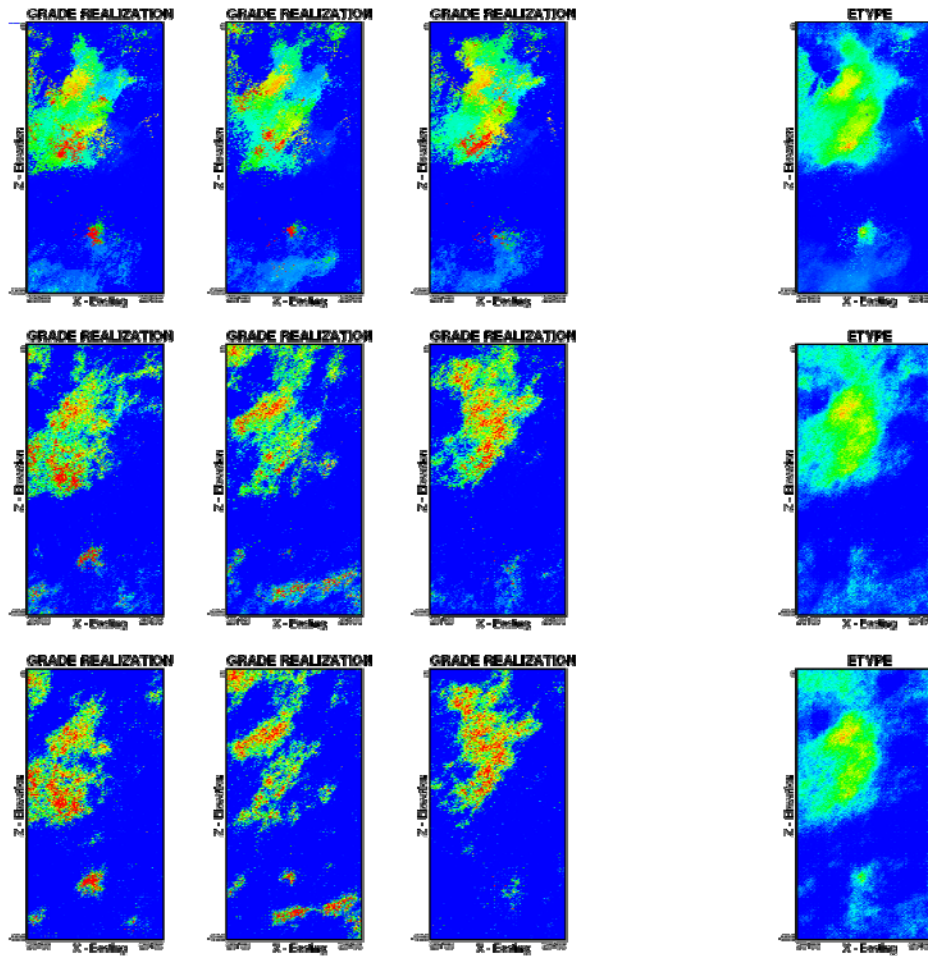
Figure 10: The first 3 SGS-LVT realizations and average over 20 realizations for the high (top row), medium (middle row), and low (bottom row) trend variability cases showing sufficient trend reproduction.